Journal of Alloys and Compounds 489 (2010) 316–323

Contents lists available at ScienceDirect

Journal of Alloys and Compounds

journal homepage: www.elsevier.com/locate/jallcom

Partial oxidation of methane over bimetallic nickel–lanthanide oxides

Ana C. Ferreira[a], A.M. Ferraria[b], A.M. Botelho do Rego[b], António P. Gonçalves[a], M. Rosário Correia[c], T. Almeida Gasche[a], Joaquim B. Branco[a,*]

[a] Instituto Tecnológico e Nuclear, Unidade de Ciências Químicas e Radiofarmacêuticas, Estrada Nacional 10, 2686-953 Sacavém, Portugal
[b] Universidade Técnica de Lisboa, IST, Centro de Química – Física Molecular and IN, Av. Rovisco Pais, 1049-001 Lisboa, Portugal
[c] Universidade de Aveiro, I3N-Departamento de Física, Campus Universitário de Santiago, 3810-193 Aveiro, Portugal

ARTICLE INFO

Article history:
Received 3 June 2009
Received in revised form 9 September 2009
Accepted 10 September 2009
Available online 23 September 2009

Keywords:
Intermetallic
Bimetallic nickel–lanthanide oxides
Methane
Partial oxidation

ABSTRACT

The study of partial oxidation of methane (POM) over bimetallic nickel–lanthanide oxides was undertaken. Binary intermetallic compounds of the type LnNi (Ln = Pr, Gd, Lu) were used as bimetallic nickel–lanthanide oxides precursors and the products ($NiO{\cdot}Pr_2NiO_4$, $2NiO{\cdot}Gd_2O_3$ and $2NiO{\cdot}Lu_2O_3$) were characterized by means of X-ray diffraction, X-ray photoelectron spectroscopy, Raman and temperature programmed reduction. The catalytic activity increases when gadolinium or lutetium replaces praseodymium and the selectivity of the bimetallic nickel–lanthanide oxides is clearly different from that of single metal oxides and/or mechanical mixtures.

The existence of an unusual synergism effect between the two metal oxide phases (NiO and Ln_2O_3) that lead to higher conversions of methane and higher selectivities to hydrogen and carbon monoxide correlate also the catalysts stability to deactivation. The activity and selectivity of the gadolinium and lutetium compounds is, under the same conditions, equivalent to that of a platinum commercial catalyst, 5 wt% Pt/Al_2O_3, which stresses the good catalytic performance of this new type of compounds for the production of H_2 and CO ($H_2/CO = 2$).

1. Introduction

The catalytic partial oxidation of methane (POM) to synthesis gas has been under intense study as a potential alternative to the highly endothermic steam reforming process. POM offers the potential for fast, efficient and economic production of synthesis gas, suitable for Fisher–Tropsch (synthetic fuels) and methanol synthesis [1–4]. Moreover, the hydrogen content can be used both in the chemical industry and for the generation of electrical energy *via* fuel cells. However, the POM reaction cannot be easily controlled due to the difficulty of removing the reaction heat from the reactor [5] and, unfortunately, the reaction is only effective at high temperatures (>700 °C), which increases the deactivation of the catalysts by carbon deposition or the sinterization of the metal active phase, especially on supported catalysts [6].

Considerable research efforts have been directed to the development of catalysts highly active and resistant to deactivation. Numerous supported metal catalysts have been used for this reaction. Among them, supported noble metals (Rh, Ru, Ir, Pt, and Pd) [7–12] and Ni [13–17] show high catalytic performance in terms of methane conversion and selectivity to synthesis gas.

Ni-based catalysts exhibit good activity and selectivity to synthesis gas formation from CH_4/O_2 mixtures and due to its low cost they were extensively studied for POM [18]. The behaviour of a number of Ni-containing catalysts, such as NiO–MgO [19], NiO–CaO [20], NiO–rare earth oxides [21–24], NiO/Al_2O_3 [25–28] and Ni-noble metals (Ru, Rh, Pt, Ir) [7–12,29] have been reported in the literature.

However, deactivation due to carbon deposition or metal loss at high temperature has been reported as a major problem for Ni catalysts. The use of Ni perovskite-type oxides seems to be a good alternative to reduce the formation and deposition of carbon on the catalysts. Choudhary et al. [30] reported that complex oxides with a perovskite structure, like $LaNiO_3$, $La_{0.8}Ca(\text{or } Sr)_{0.2}NiO_3$ and $LaNi_{1-x}Co_xO_3$ ($x = 0.2–1.0$), were resistant to coking. Tsipouriari and Verykios [31] studied POM to synthesis gas over a Ni/La_2O_3 catalyst and have found that the CH_4 conversion and the H_2 selectivity were close to thermodynamic predictions. Different additives were studied for the Ni/Al_2O_3 system [26,27,32]. Mixed metal oxides, NiO–MgO solid solutions [33], Ni–$BaTiO_3$ [34], Ni–Mg–Cr–La–O [35] and $Ni/Ca_{1-x}Sr_xTiO_3$ [36] mixed oxides, were reported to be highly active and selective catalysts at high space velocity (105–106 mL/g h) and high temperature (>700 °C) with improved coking resistance.

In this context, binary intermetallic compounds of lanthanide or actinide metals combined with *d* metals (namely Ni, Co, Mn, or Fe) have drawn the attention of many authors due to their catalytic

* Corresponding author. Tel.: +351 219946219; fax: +351 219941455.
E-mail address: jbranco@itn.pt (J.B. Branco).

0925-8388/$ – see front matter © 2009 Elsevier B.V. All rights reserved.
doi:10.1016/j.jallcom.2009.09.082

properties [37–45]. It was also observed that they decompose into oxides or nitrides responsible for their good activity and selectivity [38–40,43–49].

In our laboratories, we have using binary intermetallic compounds $LnCu_2$ (Ln = La, Ce, Pr, Nd), [38] $ThCu_2$ and $AnNi_2$ (An = U, Th) as catalytic precursors of bimetallic oxides, e.g. $3CuO{\cdot}Ln_2CuO_4$ or $2CuO{\cdot}ThO_2$ [40]. Such compounds exhibited selectivity for the 4-methylpentan-2-ol decomposition and the lanthanide-containing phase, CeO_2 or Ln_2CuO_4, seems to play a role in the formation of the CuO active sites [38]. After reduction, these bimetallic oxides were described as supported Cu catalysts on lanthanide oxides, $2Cu{\cdot}CeO_2$ and $4Cu{\cdot}Ln_2O_3$, which were active and selective for the mesityl oxide hydrogenation to 4-methylpentan-2-one (methylisobutylketone, MIKB) [49]. Their catalytic activity and selectivity was associated with the lanthanide-containing phase that seems to play an important role in the formation of the Cu or Ni active sites.

In this article, we report the results obtained for the partial oxidation of methane over Ni–lanthanide bimetallic oxides (Ln = Pr, Gd and Lu) in the temperature range 350–850 °C and at atmospheric pressure. All catalysts were characterized by powder X-ray diffraction (XRD), UV-Raman spectrometry (Raman), X-ray photoelectron spectroscopy (XPS) and temperature programmed reduction (H_2-TPR). The oxidation reaction was followed in the temperature range 350–850 °C, in the gas phase, at atmospheric pressure and the results were compared with the catalytic activity of a commercial catalyst, 5 wt% Pt/Al_2O_3.

2. Experimental

2.1. Catalysts preparation

The lanthanide intermetallic compounds, LnNi (Ln = Pr, Gd, Lu), were prepared and characterized by powder X-ray diffraction as described earlier [41].

The bimetallic Ni–lanthanide oxides were prepared by controlled oxidation of the intermetallic compounds under air (Air Liquide, O_2:N_2 = 20:80 (vol%), purity 99.995%) at 10 °C/min heating rate up to 950 °C, as described elsewhere [38].

2.2. Catalyst characterization

The XRD patterns were obtained in reflection geometry with a PANalitycal X'Pert Pro diffractometer using Cu kα monochromatic radiation (λ = 1.5406 Å). The operational settings for all scans were: voltage = 45 kV; current = 40 mA; 2θ scan range 5–80° using a step size of 0.03° at a scan speed of 0.02°/min. For identification purposes, the relative intensities (I/I_0) and the d-spacing (Å) were compared with standard JCPDS powder diffraction files [50]. The NiO, Ln_2O_3 (Ln = Gd, Lu) and Pr_2NiO_4 particle size was determined by means of the Scherrer's equation [51] using the XRD 200, 222, 222 and 111 peaks, respectively.

The XPS measurements were performed in a spectrometer XSAM800 (KRATOS) operated in the fixed analyser transmission (FAT) mode, with pass energy of 20 eV. The non-monochromatized Al Kα and Mg Kα X-radiation of 1486.6 and 1253.6 eV, respectively, were produced using a current of 10 mA and a voltage of 12 kV. Samples were analysed using 45° takeoff angle (TOA) in an ultrahigh vacuum (UHV) chamber (<10^{-7} Pa) at room temperature. Details on spectra acquisition and data treatment were published elsewhere [52]. For quantification purposes, sensitivity factors were 0.66 for O 1s, 0.25 for C 1s, 3.53 for Ni $2p_{3/2}$, 8.167 for Pr $3d_{5/2}$, 13.15 for Gd $3d_{5/2}$ and 3.83 for Lu 4d. The two first values were used as furnished by the equipment library. The other ones were obtained by multiplying the Scofield factors by the equipment response function. This last one was obtained by dividing the values furnished by the equipment library for X 1s photoelectrons (X ranging from lithium to magnesium) by the respective Scofield factors and fitting a polynomial function of kinetic energy.

The RAMAN spectra (Stokes) were obtained at room temperature in backscattering configuration with a Jobin-Yvon LabRaman HR equipped with a Multichannel air cooled (−70 °C) CCD detector. An objective of ×40 magnification was used to focus the surface of sample pellet excited with the 325 nm He–Cd laser line.

The H_2-TPR experiments were performed under pure hydrogen in an apparatus previously described [40,49]. The samples were placed in a quartz U tube (6 mm diameter), submitted to a flow of hydrogen (50 cm^3/min) under atmospheric pressure and heated up to 950 °C at a rate of 10 °C/min. The degree of reduction was determined by the quantitative analysis of water, the reduction product, as described elsewhere [53]. Prior to H_2-TPR, all samples were pretreated at 150 °C under He (F = 50 cm^3/min) during 10 min to eliminate any problem due to physisorbed water. The optimal conditions to realize good H_2-TPR experiments are found by computing the K and P parameters defined by Monti and Baiker [54] and Malet and Caballero [55], respectively. K should have a value in the range 55–140 s for $0.1 < \beta < 0.3$° s (β, heating rate) to maintain an optimal resolution. If K is lower than 55 s, the variation of hydrogen concentration is too small to be detected and if K is higher than 140 s, the hydrogen consumption is too important to consider $[H_2]$ as a constant, whereas according to Malet and Caballero [55], P values should be kept as low as possible with the upper limit of 20 °C. In this work, we decided to use the approach described by Ballivet-Tkatchenko and Delahay [56] instead of the conventional TPR analysis that uses an diluted H_2-containing mixture. This new approach enhances the sensitivity of the method as well as to perform TPR experiments under pure hydrogen. Optimized resolution was obtained by careful choice of the sample weight (≤30 mg) and hydrogen flow (F = 50 cm^3/min) taking into account the criteria established by Ballivet-Tkatchenko and Delahay [56] for the temperature programmed reduction of V_2O_5 that we have also confirmed for the reduction of CuO. The TPR curves became distorted, flat at their maximum and there is a broadening of the peaks for K > 20 s (P > 3 °C) and the optimal conditions comprise between 10–20 s and 1.5–3 °C for K and P, respectively. Under our experimental conditions, the calculated K and P values were ≈15 s and ≈ 3 °C. K is lower than 55 s which means that the variation of hydrogen concentration should be too small to be detected. However, using the analysis of water evolution this problem is avoided and the hydrogen concentration can be better considered as constant and it is possible to perform TPR experiments under pure hydrogen without possible kinetic problems ascribed to the use of low hydrogen concentrations. Our P value (3 °C) is also much lower than 20 °C, which confirm that our H_2-TPR experimental standard conditions are adequate to maintain good resolution. Water was analysed on a Shimadzu 9A instrument equipped with thermal conductivity detector (TCD), helium was used as carrier gas (F = 50 cm^3/min, $T_{Detector}$ = 105 °C, 150 mA), connected to a CR3 Shimadzu integrator.

2.3. Catalytic activity

The catalytic partial oxidation of methane was carried out at atmospheric pressure in a fixed-bed U-shaped quartz reactor, plug-flow type reactor, with a quartz frit and an inside volume of 15 cm^3. Mass flow controllers were used to control CH_4 (Air Liquide, purity 99.9995%), air (Air Liquide, purity 99.9995%) and He (Air Liquide, purity 99.9995%) flows. A thermocouple was placed near the catalytic bed for continuous monitoring of the sample temperature. Unless otherwise stated, a gaseous mixture of CH_4 (28%), O_2 (14%) and N_2 (58%) was introduced and the reaction was studied with an adequate gas hourly space velocity (GHSV, mL of CH_4/g of catalyst h) of 8500, m = 100 mg. The outlet gas was cooled in an ice-water trap and its composition analysed on-line by gas chromatography using a Restek ShinCarbon ST column (L = 2.0 m, ϕ = 1/8 in., ID = 1 mm, 100/200 mesh) and an Agilent 4890D GC equipped with a thermal conductivity detector (TCD) and a 6-port gas sampling valve with a 0.250 μL loop.

Catalyst activity (r_i) was defined as the number of mL of methane converted per gram of catalyst and per hour (mL_{CH4}/g h). The conversion of methane, the selectivity and the yield of the products were calculated as follows: $Conv._{CH_4}$ (%) = $\{([CH_4]_i - [CH_4]_o)/[CH_4]_i\} \times 100$; $Sel._{CO}$ (%) = $\{[CO]_o/([CH_4]_i - [CH_4]_o)\} \times 100$; $Sel._{CO_2}$ (%) = $\{[CO_2]_o/([CH_4]_i - [CH_4]_o)\} \times 100$ and $Sel._{H_2}$ (%) = $\{[H_2]_o/2 \times ([CH_4]_i - [CH_4]_o)\} \times 100$, where $[CH_4]_i$ are inlet flow rates, and $[CH_4]_o$, $[CO]_o$, $[CO_2]_o$, and $[H_2]_o$ are outlet flow rates. The amount of reagents and products was confirmed by an external standard method using reference mixtures of CH_4, CO, CO_2 and H_2 (Air Liquide). The confidence level was better than 95%. Unless otherwise stated, the values reported in this paper represent the initial activities of the catalysts after 1 h on stream. The catalysts activity was compared to that of a commercial catalyst (5.0 wt% Pt/Al_2O_3, Aldrich), one standard in this research field [1].

3. Results and discussion

3.1. Catalysts characterization

Fig. 1 shows the diffraction patterns obtained before catalytic tests for the Ni–lanthanide oxides LnNiOx (Ln = Pr, Gd and Lu). As can be seen, the patterns were consistent with those of standard NiO, Pr_2NiO_4, Gd_2O_3 and Lu_2O_3 cubic phases as reported on the standard JCPDS powder diffraction files [50], with a nearly absence of differences in the respective lattice parameters.

The average particle size was estimated from the half-width of the NiO (200), Pr_2NiO_4 (200) and Ln_2O_3 (222) diffraction peaks using the Scherrer's equation. The values obtained were close to each other for all the samples: ≈60–80 nm.

To characterize the surface elemental composition as well as the oxidation states, samples were analysed by XPS. O 1s, Ni 2p, Pr 3d Gd $3d_{5/2}$ and Lu 4d were the main studied regions. Also the C 1s region was acquired for binding energy reference pur-

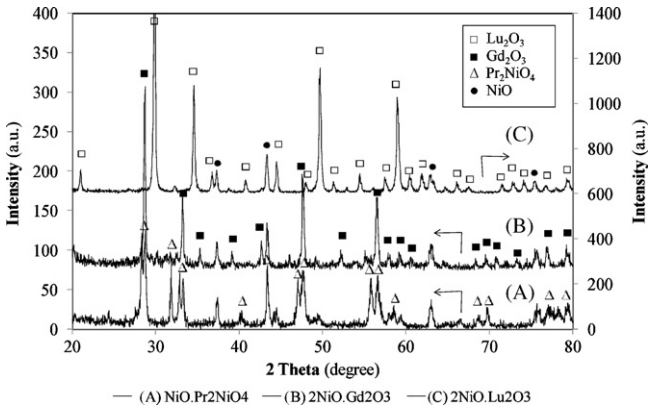

Fig. 1. XRD patterns for the Ni–lanthanide oxides before reaction.

poses. The XPS regions for the lanthanide elements are shown in Fig. 2.

Binding energies for Pr $3d_{5/2}$, Gd $3d_{5/2}$ and Lu $4d_{5/2}$ are 933.2, 1187.5, 196.3 eV, respectively, which confirm that the lanthanides are present, at least in the surface, within the thickness probed by XPS, under the form of Ln^{3+} [57].

On the other hand, the Ni 2p spectra show that the surfaces of the Ni–lanthanide oxides LnNiOx (Ln = Pr, Gd and Lu) exhibit components assignable to nickel hydroxide (Fig. 3). However, we cannot completely discard the presence of Ni in the 3+ state due to the formation of nickel oxyhydroxides (NiOOH) that are reported to have a binding energy of 855.9 ± 0.1 eV [58], close to the shoulder in the NiO spectrum and to the binding energy for $Ni(OH)_2$ (854.6 eV) [59]. The peak due to presence of Ni^0 species (around 852.6 eV) was not detected.

Other important information can be inferred from the O 1s core level spectrum. Fig. 4 shows that all Ni–lanthanide oxides spectra have three distinct components. They are centred at 529.4, 531.5 and 532.4 eV and are assignable, respectively, to oxide, to hydroxide and to adsorbed oxygen under the form of O and/or O_2 [60] or under the form of carbonate ion on the samples surface.

Table 1 presents the quantitative results for samples before catalytic tests.

From the quantitative point of view, the atomic ratio Ln/Ni is, at least at the surface, always larger than the expected one (=1) and compatible with a positive superficial segregation of the lanthanide. Moreover, the amount of oxygen assignable to oxides is in excess if we consider that all the Ni should be under the form of NiO (no metallic Ni was found) and all the lanthanides should be under the form of Ln_2O_3. This favours the hypothesis that some of the superficial nickel is in an oxidized form (hydroxide, oxyhydroxide). However, it has been also shown that, for a binary alloy, the element with the larger atomic radius and higher reactivity with the ambient (i.e. higher heat of formation of metal oxide) will segregate to the surface (ΔH_f $Lu_2O_3 = -1878$, $Gd_2O_3 = -1819$; $Pr_2O_3 = -1809$; $Ni_2O_3 = -489$ kJ/mol) [61–64]. Therefore, at least a part of the quantified excess of oxygen may be due to the segregation of lanthanide to the surface (quantifications are performed assuming that a homogeneous elemental distribution in depth exists). Since the samples are powders, no further exploitation of data (angular resolution, for instance) is possible. Thence, the following tentative surface compositions can be written: $(NiO)(Pr_2O_3)_{1.05}$, $(NiO)(Gd_2O_3)_{0.85}$ and $(NiO)(Lu_2O_3)_{2.15}$.

In order to investigate the catalyst further, temperature-programmed reduction studies were performed. Typical H_2-TPR profiles obtained for the nickel–lanthanide oxides are shown in Fig. 5.

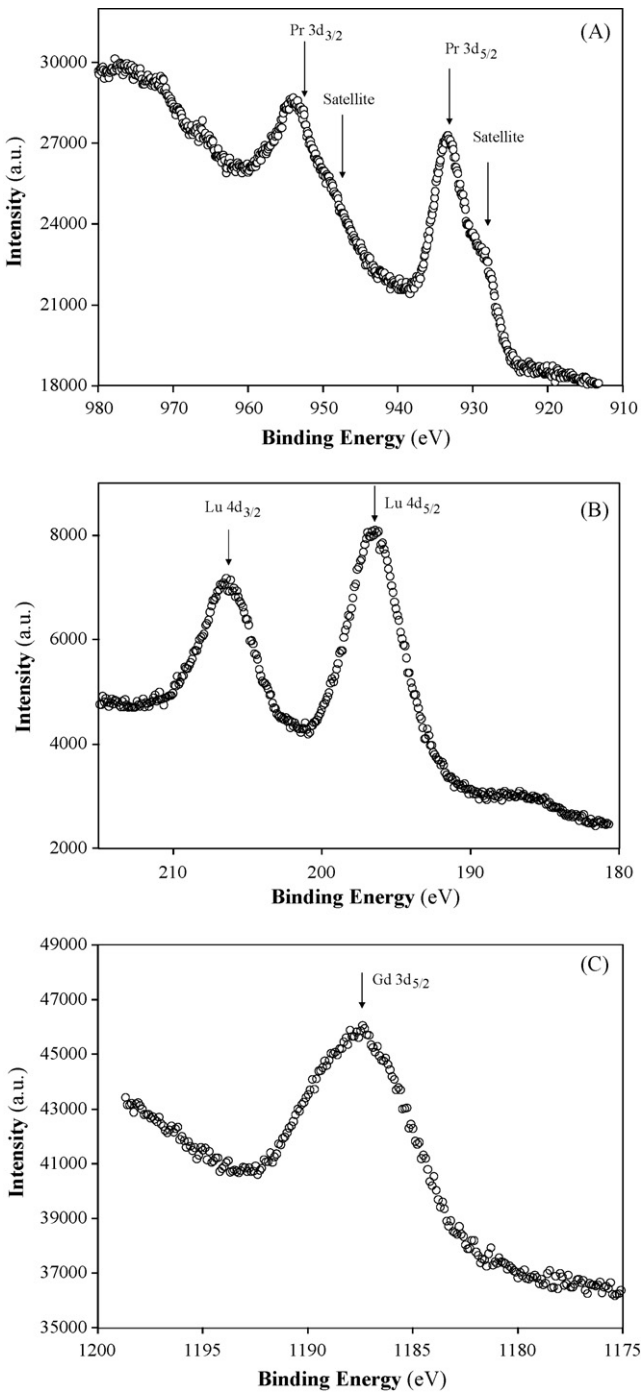

Fig. 2. XPS regions showing the lanthanide regions of (A) Pr 3d; (B) Lu 4d and (C) Gd $3d_{5/2}$.

The H_2-TPR profiles exhibit one reduction peak in the temperature range studied (20–1000 °C), except for the compound of praseodymium that shows two reduction peaks. The temperature at maximum water evolution rate (T_m) shifts to higher temperature when Pr is replaced by Lu and Gd (found T_m, 337, 347 and 357 ± 5 °C, respectively), whereas for the second mass loss of the Pr compound, the T_m is much higher (532 ± 5 °C). The T_m for pure NiO is always lower (295 ± 5 °C) but, in agreement with published values for the reduction of nickel oxide [40,54].

The H_2-TPR quantitative analysis of water produced on each mass loss gives a H_2O:Ln molar ratio of 1.7, 2.3 and 2.1 ± 0.2 for the first mass losses of the Pr, Gd and Lu bimetallic oxides, respec-

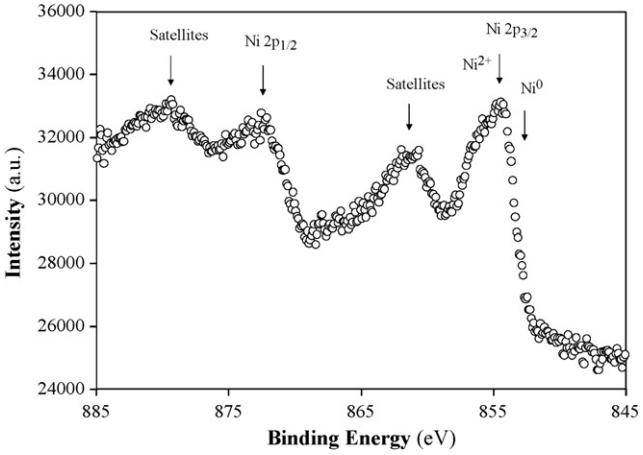

Fig. 3. XPS Ni 2p region for the bimetallic Ni–Gd oxide.

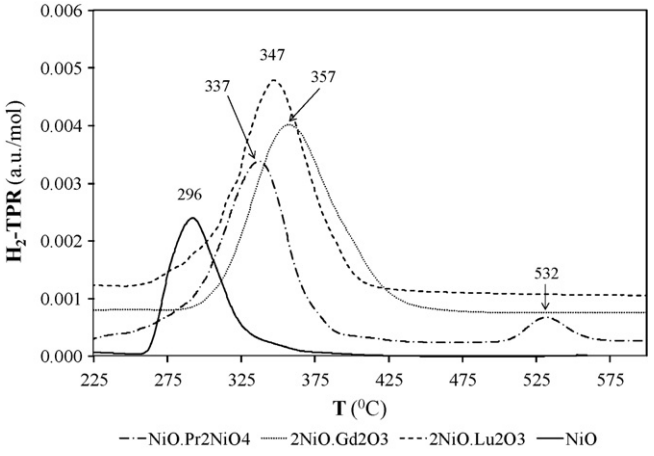

Fig. 5. H_2-TPR profiles under pure hydrogen.

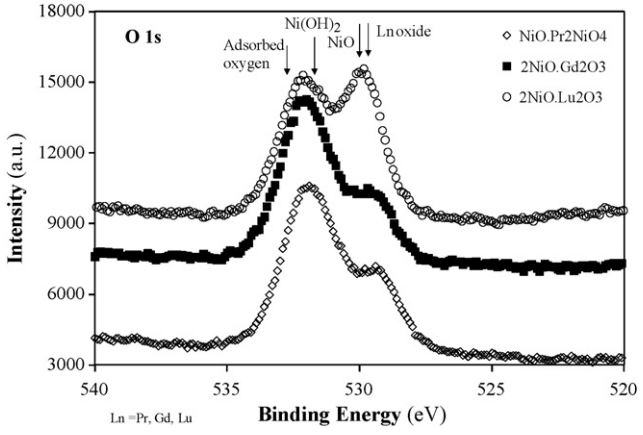

Fig. 4. XPS O 1s region for the three bimetallic Ni–lanthanide oxides.

tively, whereas the Ni–Pr bimetallic oxide has associated with the second mass loss a H_2O:Pr molar ratio of 0.2 ± 0.1. After the H_2-TPR studies, the XRD patterns of the reduced samples show pure crystalline phase of metallic Ni along with Ln_2O_3 (Ln = Pr, Gd, Lu) (Fig. 6).

To understand such results we must take into account that the standard enthalpy and Gibbs free energy for the reduction of NiO is considerably more favourable than that of the lanthanide oxides (Ln_2O_3, Ln = Pr, Gd) (e.g. $\Delta_f G^\circ = -16.87$ kJ/mol for the reduction of NiO and +1591.03 kJ/mol for the reduction of Gd_2O_3) [64,65]. In the case of Pr_2NiO_4, to the best of our knowledge, only the enthalpy of formation ($\Delta_f H^\circ$) is known from the literature [66]. Nevertheless, the entropic factor has, for the reduction of NiO and Ln_2O_3, a positive sign, and the main contribution for the Gibbs free energy of solids is due to the gases (H_2 and H_2O) produced during the reduction [64]. Therefore, in the case of the reduction of Pr_2NiO_4 the enthalpy of reduction is a good measure of their stability (+52.28 kJ/mol for the reduction of Pr_2NiO_4 into Pr_2O_3), which explains the second reduction peak at higher temperature.

Thus, the reduction of NiO is expected at first and a common step can be assigned to the reduction of the heterobimetallic Ni–lanthanide oxides, whereas in the case of the Ni–Pr bimetallic oxide the existence of a second reduction step can be attributed to the reduction of the ternary oxide phase and formation of Pr_2O_3.

On the other hand, the T_m values for the reduction of the Ni–lanthanide heterobimetallic NiO species were higher than that of pure NiO, instead of lower. This can be attributed to a form of stable nickel oxide (oxygen less labile) more difficult to reduce than pure NiO and due to interaction with the lanthanide containing phases. Gervasini and co-workers [67] proposed the same explanation for the hindered reduction of nano-sized CuO dispersed on synthesized silica modified with alumina, titania and zirconia. Furthermore, the obtained results for evolution of T_m when Gd or Lu substitutes Pr indicate that the lanthanide-containing phase seems to play a role on the reduction of the bimetallic Ni–lanthanide oxides but, to obtain a trend of evolution, this work needs to be enlarged to the all lanthanide series.

Therefore, the reduction behaviour of the bimetallic Ni–lanthanide oxides seems to be determined by the existence of unusual stable NiO particles modified by the interaction with the lanthanide oxide phase that hinders their reduction. As previously reported, bulk diffusion of Ni atoms in lanthanum oxide perovskite type structure catalysts, $LaNiO_3$, is inhibited as a consequence of the physical barriers established by the La_2O_3 particles [17]. Moreover, the metallic Ni crystallites maintain a

Table 1
XPS quantitative results for Ni–lanthanide oxides in atomic %.

Lanthanide	Pr	Gd	Lu
O 1s [a]	82.1 (22.8)	88.0 (20.9)	79.4 (40.5)
Ni $2p_{3/2}$	5.9	4.4	3.9
Pr $3d_{5/2}$	12.0		
Gd $3d_{5/2}$		7.6	
Lu 4d			16.7
Ln/Ni	2.1	1.7	4.3

[a] Total O 1s % (O^{2-} %).

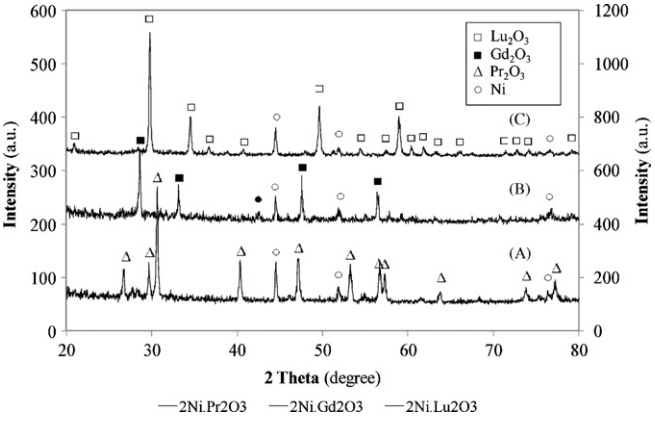

Fig. 6. XRD patterns after H_2-TPR.

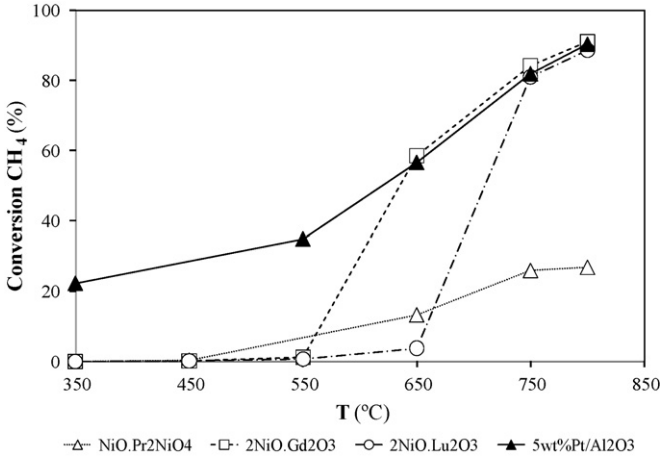

Fig. 7. Temperature effect on the conversion of methane over the bimetallic Ni–lanthanide oxides, NiO and 5 wt% Pt/Al_2O_3.

good dispersion on the La_2O_3 surface and the good stability of the catalyst is mainly due to the ability to stabilize the Ni crystallites in a high dispersion degree on a La_2O_3 matrix, thus limiting the extent of metallic particles sintering.

3.2. Catalysts activity and stability

The bimetallic Ni–lanthanide oxides were active and selective for the partial oxidation of methane. Fig. 7 shows the effect of the temperature on their catalytic performance in the temperature range studied, 350–800 °C, under a molar ratio of $CH_4/O_2 = 2$. For comparison purposes, the behaviour of a commercial platinum catalyst, 5 wt% Pt/Al_2O_3, was also studied under the same experimental conditions.

The conversion of CH_4 increases with the temperature of reaction. At 800 °C, the order of activity is as follows: NiO (46%), Pr–Ni oxide (27%), Gd–Ni oxide (91%) and Lu–Ni oxide (89%), which for the Gd and Lu compounds is two times superior to that of pure NiO (for clarity purposes, not shown in Fig. 7). Moreover, the behaviour of the Gd–Ni oxide at $T \geq 650$ °C and that of the Lu–Ni oxide at $T \geq 750$ °C is comparable to that of a commercial catalyst of platinum on alumina, 5 wt% Pt/Al_2O_3.

Fig. 8 shows the evolution of the catalysts selectivity to hydrogen and carbon dioxide with the temperature of reaction. The production of H_2 increases with the temperature, whereas the production of CO_2 decreases significantly and becomes residual at $T \geq 750$ °C (<1%), except for the Pr compound. The other products detected were carbon monoxide that increases with the temperature and C2 hydrocarbons (ethylene and ethane) that were only detected on Pr–Ni oxide and at very low concentrations (≤1%, $T \geq 750$ °C). The results obtained on Gd and Lu–Ni oxides were again very similar to those obtained on the platinum commercial catalyst.

After analysis of the catalytic performance of the bimetallic Ni–lanthanide oxides, it can be said that the rare earth influence the activity and selectivity of the reaction in terms of a small effect when Lu substitutes Gd.

The nickel–lanthanide oxide catalysts were also stable for at least 16 h of time on stream, at each temperature studied (500, 600, 700, 750 and 800 °C), which correspond to an overall time of 96 h. Other authors have used periods of 6–16 h to study the evolution of the catalysts activity/selectivity [22,68]. As an example, Fig. 9 shows the conversion of methane and the selectivities to CO, H_2 and CO_2 over the Gd–Ni oxide catalyst as a function of the time on stream at 750 °C. The conversion of methane was constant ≈84%, whereas the selectivities to CO and H_2 remained stable at

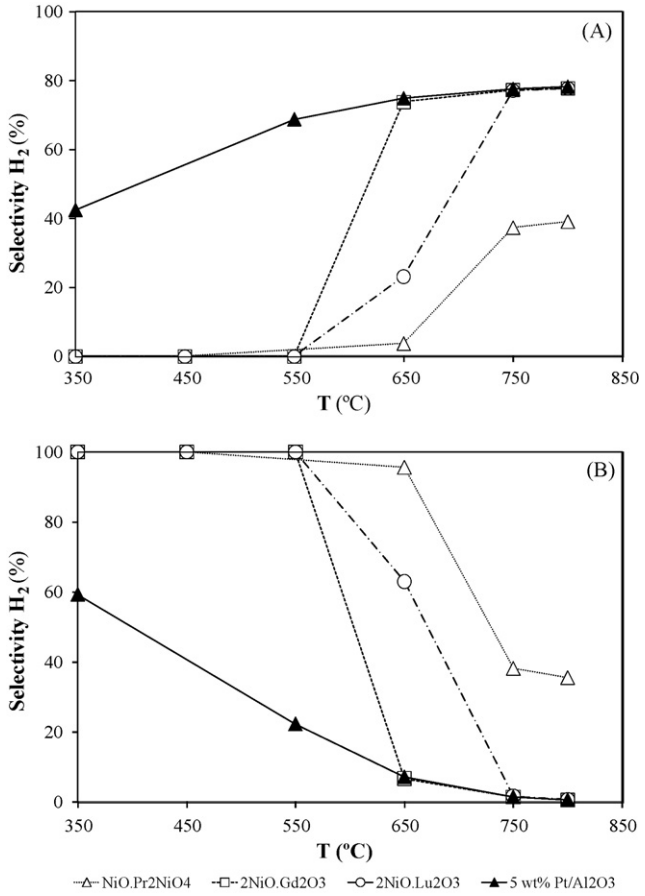

Fig. 8. Temperature effect on the selectivity to H_2 (A) and CO_2 (B) over the bimetallic Ni–lanthanide oxides, NiO and 5 wt% Pt/Al_2O_3.

≈22 and ≈77%, respectively; the formation of CO_2 was residual (<1%).

To our knowledge, this is the first time that such results are reported using binary intermetallic compounds of the type LnNi (Ln = Pr, Gd and Lu) as bimetallic oxide precursors, which stresses the advantage of this synthetic route.

This raises the question about the nature of the active sites for the catalytic POM over Ni–lanthanide oxides and the roles played by Ni and lanthanide oxides on their formation. NiO and the lanthanide

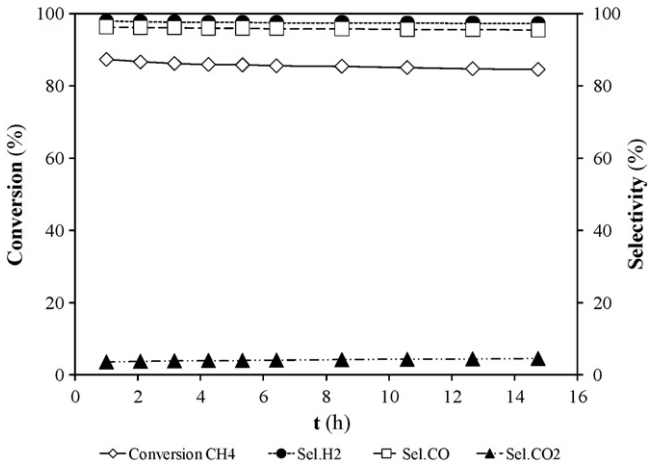

Fig. 9. Partial oxidation of methane over the bimetallic Ni–Gd oxide as a function of time on stream at 750 °C.

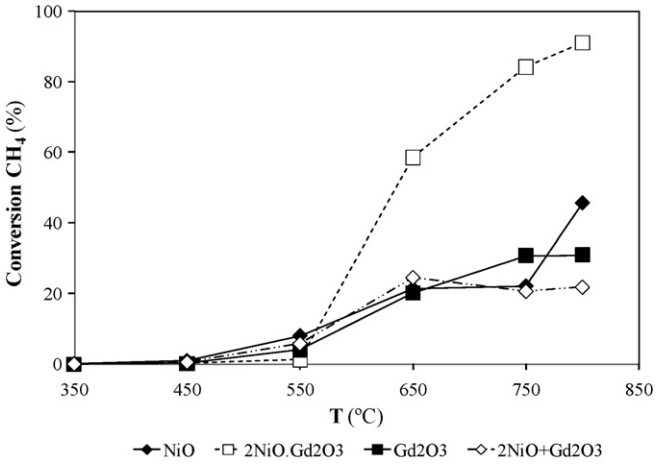

Fig. 10. Temperature effect on the conversion of methane over the NiO, Gd_2O_3 mechanic mixture of $2NiO + Gd_2O_3$ and the bimetallic Ni–Gd oxide.

oxides are catalytically active for the oxidation of methane oxides [21–24,69,70], which was confirmed by our results. However, their catalytic behaviour is clearly different from that of the corresponding Ni–lanthanide bimetallic oxides reported in this work. As an example, Fig. 10 shows the comparison of the activity of NiO and Gd_2O_3 with that of the Ni–Gd bimetallic oxide.

The catalytic activity of the Ni–lanthanides bimetallic oxides is very different from that of the pure metal oxides; which is confirmed by the differences in the evolution of the selectivities with the temperature (Fig. 11). Therefore, if NiO and the lanthanide oxides have a role in the catalytic process, these differences can only be ascribed to the existence of an unusual synergism effect between the two metal oxide phases in the Ni–lanthanide bimetallic oxides.

In order to explain our results and to approach the true nature of the active sites, the analysis of the catalysts after reaction was undertaken. After reaction, the formation of other oxide phases that could correspond to the formation of new solid solutions between NiO and the lanthanide oxide phase were not detected but, the appearance of Ni due to NiO total reduction could be identified by XRD (Fig. 12). The appearance of Ni was especially important for the Gd and Lu samples, whereas the diffraction patterns of the NiO phase were undetected by XRD. The average particle size, determined by the Scherrer's equation, were comparable to those obtained before reaction.

In addition, changes were also observed in the bimetallic Gd–Ni and Lu–Ni oxides Raman spectra obtained before and after the reaction, which is not the case in the Pr–Ni oxide spectrum (Fig. 13). In all the cases, a blue shift and a decreasing on the full width half maxima of the spectral lines after reaction are observed.

The Pr–Ni oxide presents similar Raman spectra after and before the reaction. There is a weak broad peak at ~384 cm^{-1}, but it is lower than the wave number of the strongest Raman line expected for the predictable Ni–O stretching peak (~450 cm^{-1}) either in stoichiometric or oxidized $Pr_2NiO_{4+\delta}$ samples or even for the Ln–O stretching vibration (~406 cm^{-1}) on the Pr_2O_3 trigonal A-type [71]. As the synthesis of the catalysts takes place in a rich oxygen atmosphere it is most probable that this peak corresponds to point defects, such as interstitial oxygen ions, as has been reported in the literature [72]. The weak shoulder observed at ~600 and ~800 cannot be unambiguously assigned to any of the NiO, $Pr_2NiO_{4+\delta}$ or Pr_2O_3 compounds. From the Raman spectra it is evident the poor crystalline structure of the Pr–Ni oxide phases formed.

The more significant spectral changes are observed for the Ga–Ni and Lu–Ni oxide samples, where new spectral features arise above and below the band at ~344 and ~377 cm^{-1}, respectively. Lan-

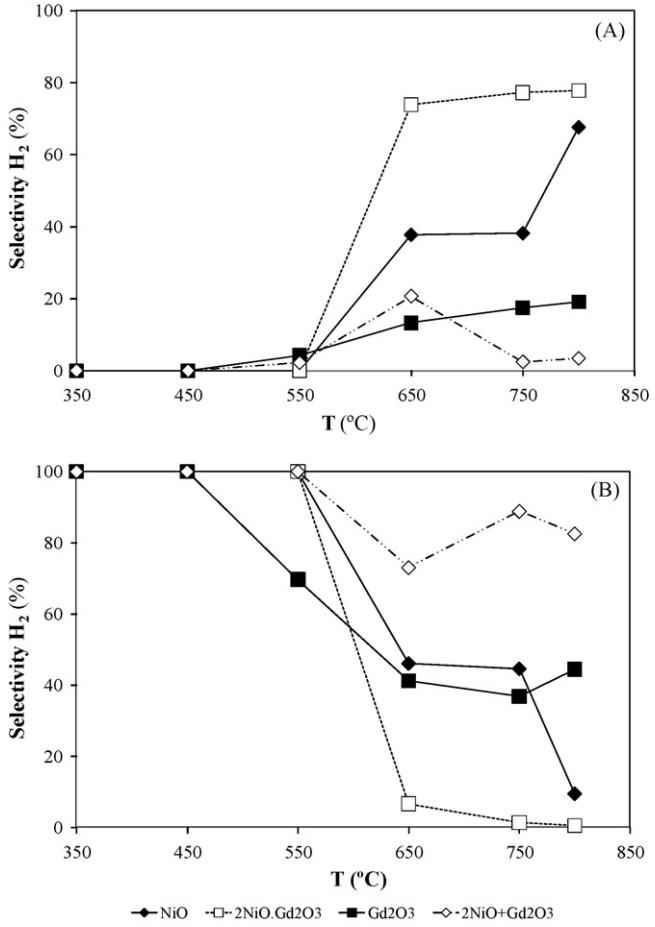

Fig. 11. Temperature effect on the selectivity to H_2 (A) and CO_2 (B) over NiO, Gd_2O_3 mechanic mixture of $2NiO + Gd_2O_3$ and the bimetallic Ni–Gd oxide.

thanides sesquioxides are known to crystallize in various structures according to the radius of the rare earth ion [73]. The Gd_2O_3 crystallize in cubic phase at 650 °C and the monoclinic and cubic phases are simultaneously present in samples annealed at 800 and 900 °C [74]. Before reaction, for the spectral region between 200 and 1200 cm^{-1}, the main strongest Raman lines (P_C) are located at 344 cm^{-1} and 373 cm^{-1}, for Ga and Lu oxides respectively, following the trend expected with the decreases on the lanthanides ionic radius [71]. However, this value is lower than the expected (361 cm^{-1}) for the

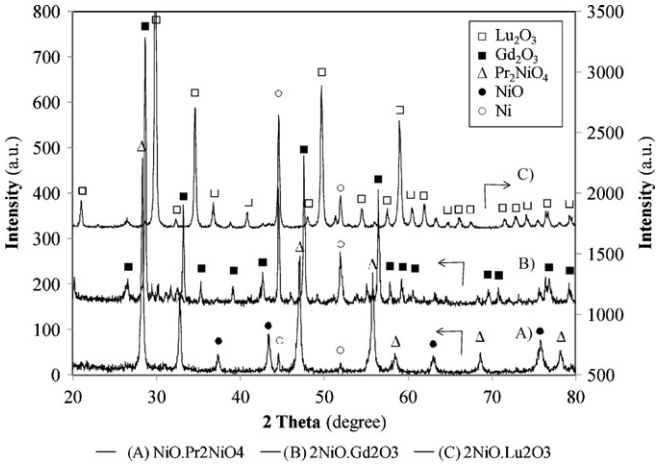

Fig. 12. XRD patterns for the bimetallic Ni–lanthanide oxides after reaction.

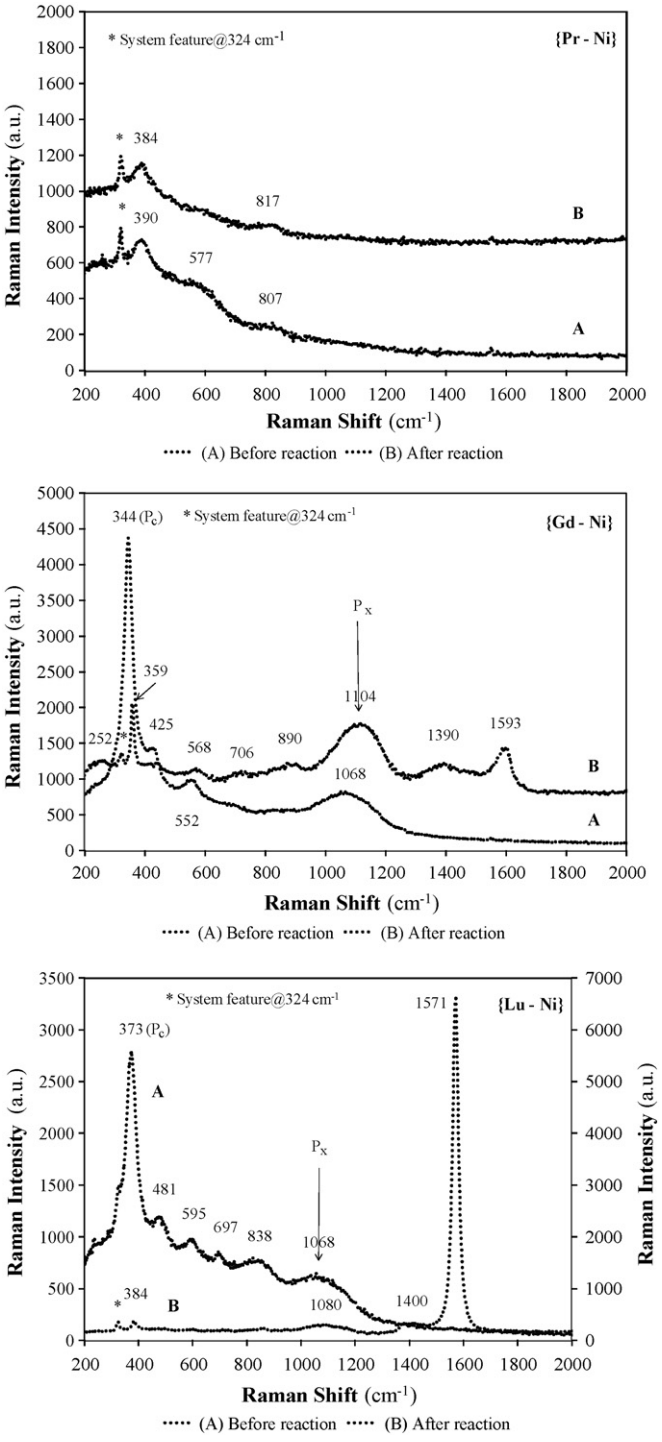

Fig. 13. Raman spectra at room temperature for bimetallic Ni–lanthanide oxides when excited with the HeCd 325 nm laser line.

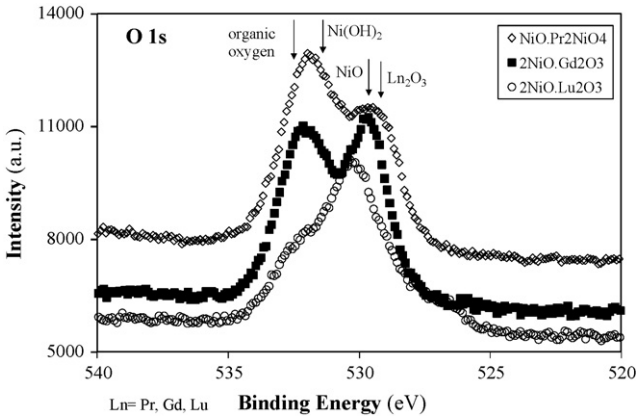

Fig. 14. XPS O 1s region for the three bimetallic Ni–lanthanide oxides after the catalytic reaction.

strongest peak in cubic C-type or monoclinic B-type (385 cm^{-1}) Gd_2O_3 [74] and C-type Lu_2O_3 (390 cm^{-1}) [75]. The lower value of this Raman peak before reaction may be related with the presence of the Ni cation of the NiO oxide which induces an expanded Ln_2O_3 structure [72]. After reaction, the position of this peak shifts to the value expected for the C-type Gd_2O_3 and Lu_2O_3 phase, which can be attributed to an annealing effect during the reaction with CH_4 [74].

Above the first Raman spectral region comes up a broad band located between 1000 and 1100 cm^{-1} (PX). This band arises when the Gd and Lu substitute Pr, and after reaction its intensity increases in relation to the strongest peak in the Raman first order region. The presence of this band correlates well with the increasing of the catalytic performance of Gd and Lu oxides, relatively to that obtained with Pr oxides. After reaction the intensity ratios I_{PX}/I_{PC} increase ~40× in both cases. The origin of this band is either due to the defects or to a point defect that originates a local vibration, such as metal–oxygen–vacancy complexes [73]. Since oxygen vacancies are active sites for combustion reactions, this finding confirm the bimetallic Ni–lanthanide oxides, particularly in the cases of Gd and Lu, good catalytic behaviour for POM. Moreover, after reaction, and only when the Pr is replaced by Gd and Lu, the spectra have a typical shape of graphitic/DLC films containing contributions from the G vibrational mode of graphite, involving E_{2g} symmetrical bond stretching motion of pairs of sp^2 carbon atoms, and the D band associated with the breathing mode of six-membered rings [76].

The absence of the typical shape of graphitic/DLC films for the Pr oxides is in good agreement with the lower catalytic performance obtained for this lanthanide.

Finally, the XPS Ni 2p spectra for all the samples are very similar before and after reaction and do not show any metallic Ni at the surface after the reaction. Additionally, no changes on the XPS spectra are observed for the main peaks of the rare earth components ($3d_{5/2}$ for Pr and Gd, and $4d_{5/2}$ for Lu) and it can be said that the oxidation state of the rare earths is the same before and after the catalytic reaction (Ln^{3+}). Nevertheless, a major difference emerges when we compare the XPS quantitative analysis data before and after reaction: the atomic ratio Ln/Ni decreases for all samples (from 2.1 to 1.6 for Ln = Pr; from 1.7 to 0.6 for Ln = Gd; from 4.4 to 2.9 for Ln = Lu.) confirming the increase of Ni at the catalysts surface after reaction. The other significant difference emerges from the XPS O 1s spectra obtained for the bimetallic Ni–lanthanide oxides after reaction (Fig. 14), where the relative importance of O^{2-} (lowest binding energy) component increases.

Choudhary et al. [22] investigated the selective oxidation of methane to CO and H_2 over NiO-rare earth oxide catalysts and conclude that the degree of reduction of the catalysts was an important factor governing inherent catalysts activity and selectivity. The conversion increases on the reduced catalysts as compared to the unreduced catalysts. The formation of coke on catalysts harmless to their catalytic activity/selectivity was also observed earlier and has been attributed to the Boudouard reaction [22,68].

In conclusion, despite of the carbon deposition on the catalysts surface, the catalytic activity/selectivity is not affect and the bimetallic Ni–lanthanide oxides good activity and selectivity correlate the increase of nickel and oxygen at the catalysts surface. An unusual interaction between nickel and lanthanide in the

nickel–lanthanide oxides could also contribute to the bimetallic nickel–lanthanide oxides good catalytic behaviour but, additional studies have to be performed in a nearly future.

4. Conclusions

The results obtained in the present work show that the bimetallic Ni–lanthanide oxide catalysts obtained by an intermetallic route via oxidation of LnNi (Ln = Pr, Gd, Lu) were very active and selective for the partial oxidation of methane and production of synthesis gas. The catalytic performance of the Ni–lanthanide oxides increases when Gd or Lu substitutes Pr, which seems to indicate that the catalysts behaviour depends on the lanthanide-containing phase. The activity and selectivity of the Gd and Lu compounds was, under the same conditions, comparable to that of a platinum commercial catalyst, 5 wt% Pt/Al_2O_3, which stresses the good catalytic performance of this new type of compounds.

Acknowledgments

This work was supported by the Portuguese "Fundação para a Ciência e a Tecnologia" under the contract PTDC/EQU-EQU/65126/2006.

References

[1] D.A. Hickman, L.D. Schmidt, Science 259 (1993) 343–346.
[2] D. Dissanayake, M.P. Rosynek, K.C.C. Kharas, J.H. Lunsford, J. Catal. 132 (1991) 117–127.
[3] A.P.E. York, T.C. Xiao, M.L.H. Green, Top. Catal. 22 (2003) 345–358.
[4] S. Freni, G. Calogero, S. Cavallaro, J. Power Sources 87 (2000) 28–38.
[5] S.L. Liu, G.X. Xiong, H. Dong, W.S. Yang, Appl. Catal. A 202 (2000) 141–146.
[6] M. Matsukata, T. Matsushita, K. Ueyama, Chem. Eng. Sci. 51 (1996) 2769–2774.
[7] R. Horn, K.A. Williams, N.J. Degenstein, A. Bitsch-Larsen, D.D. Nogare, S.A. Tupy, L.D. Schmidt, J. Catal. 249 (2007) 380–393.
[8] E.P.J. Mallens, J.H.B.J. Hoebink, G.B. Marin, J. Catal. 167 (1997) 43–56.
[9] A. Donazzi, A. Beretta, G. Groppi, P. Forzatti, J. Catal. 255 (2008) 241–258.
[10] S. Rabe, M. Nachtegaal, F. Vogel, Phys. Chem. Chem. Phys. 9 (2007) 1461–1468.
[11] P. Gelin, M. Primet, Appl. Catal. B-Environ. 39 (2002) 1–37.
[12] K. Sekizawa, H. Widjaja, S. Maeda, Y. Ozawa, K. Eguchi, Catal. Today 59 (2000) 69–74.
[13] V.A. Tsipouriari, Z. Zhang, X.E. Verykios, J. Catal. 179 (1998) 283–291.
[14] V.R. Choudhary, V.H. Rane, A.M. Rajput, Appl. Catal. A 162 (1997) 235–238.
[15] J. Barbero, M.A. Pena, J.M. Campos-Martin, J.L.G. Fierro, P.L. Arias, Catal. Lett. 87 (2003) 211–218.
[16] Y. Zhang, Z.X. Li, X.B. Wen, Y. Liu, Chem. Eng. J 121 (2006) 115–123.
[17] M.E. Rivas, J.L.G. Fierro, R. Guil-Lopez, M.A. Pena, V. La Parola, M.R. Goldwasser, Catal. Today 133 (2008) 367–373.
[18] T.L. Zhu, M. Flytzani-Stephanopoulos, Appl. Catal. A 208 (2001) 403–417.
[19] V.R. Choudhary, A.S. Mamman, S.D. Sansare, Angew. Chem.-Int. Ed. 31 (1992) 1189–1190.
[20] V.R. Choudhary, A.M. Rajput, B. Prabhakar, Catal. Lett. 15 (1992) 363–370.
[21] S. Xu, X.B. Yan, X.L. Wang, Fuel 85 (2006) 2243–2247.
[22] V.R. Choudhary, V.H. Rane, A.M. Rajput, Catal. Lett. 22 (1993) 289–297.
[23] A. Djaidja, A. Barama, M.M. Bettahar, Catal. Today 61 (2000) 303–307.
[24] V.R. Choudhary, A.M. Rajput, V.H. Rane, Catal. Lett. 16 (1992) 269–272.
[25] V.R. Choudhary, A.M. Rajput, B. Prabhakar, J. Catal. 139 (1993) 326–328.
[26] Q. Miao, G.X. Xiong, S.S. Sheng, W. Cui, L. Xu, X.X. Guo, Appl. Catal. A 154 (1997) 17–27.
[27] L. Cao, Y. Chen, W. Li, Natural Gas Conversion IV, vol. 107, 1997, pp. 467–471.
[28] Q.G. Yan, W. Chu, L.Z. Gao, Z.L. Yu, S.Y. Yuan, Natural Gas Conversion V, vol. 119, 1998, pp. 855–860.
[29] A. Donazzi, A. Beretta, G. Groppi, P. Forzatti, J. Catal. 255 (2008) 259–268.
[30] V.R. Choudhary, B.S. Uphade, A.A. Belhekar, J. Catal. 163 (1996) 312–318.
[31] V.A. Tsipouriari, X.E. Verykios, J. Catal. 179 (1998) 292–299.
[32] W. Chu, W.G. Yan, X. Liu, Q. Li, Z.L. Yu, G.X. Xiong, Natural Gas Conversion V, vol. 119, 1998, pp. 849–854.
[33] S. Tang, J. Lin, K.L. Tan, Catal. Lett. 51 (1998) 169–175.
[34] R. Shiozaki, A.G. Andersen, T. Hayakawa, S. Hamakawa, K. Suzuki, M. Shimizu, K. Takehira, J. Chem. Soc., Faraday Trans. 93 (1997) 3235–3242.
[35] P. Chen, H.B. Zhang, G.D. Lin, K.R. Tsai, Appl. Catal. A 166 (1998) 343–350.
[36] T. Hayakawa, H. Harihara, A.G. Andersen, K. Suzuki, H. Yasuda, T. Tsunoda, S. Hamakawa, A.P.E. York, Y.S. Yoon, M. Shimizu, K. Takehira, Appl. Catal. A 149 (1997) 391–410.
[37] J.S. Abell, in: K.A.G. Jr., E. LeRoy (Eds.), Handbook on the Physics and Chemistry of Rare Earth, North-Holland Publishing Company, Amsterdam, 1989, p. 1.
[38] D. Ballivet-Tkatchenko, J. Branco, A.P. Dematos, J. Phys. Chem. 99 (1995) 5481–5484.
[39] J.B. Branco, D. Ballivet-Tkatchenko, A. Pires de Matos, J. Mol. Catal. A, Chemical 307 (2009) 37–42.
[40] J. Branco, C. de Jesus Dias, A.P. Goncalves, T.A. Gasche, A.P. de Matos, Thermochim. Acta 420 (2004) 169–173.
[41] J.B. Branco, T.A. Gasche, A.P. Goncalves, A.P. de Matos, J. Alloys Compd. 323 (2001) 610–613.
[42] K.H.J. Buschow, in: K.A.G. Jr., E. LeRoy (Eds.), Handbook on Physics and Chemistry of Rare Earth, North-Holland Publishing Company, Amsterdam, 1984, p. 1.
[43] A. Iandelli, A. Palenzona, in: K.A.G. Jr., E. LeRoy (Eds.), Handbook on the Physics and Chemistry of Rare Earth, North-Holland Publishing Company, Amsterdam, New York, Oxford, 1979, pp. 1–54.
[44] G. Sandrock, S. Suda, L. Sclapbach, in: L. Sclapbach (Ed.), Topics in Applied Physics, Springer-Verlag, Berlin, Heidelberg, New York, 1992, pp. 197–258.
[45] W.E. Wallace, J. France, A. Shamsi, in: G.J. MaCarthy, J.J. Rhyne, H.S. Silber (Eds.), Catalysis using Rare Earth and Actinide Intermetallics, Plenum Press, New York, London, 1982, p. 561.
[46] G.B. Atkinson, E.G. Baglin, L.J. Nicks, D.J. Bauer, in: R.G. Herman (Ed.), Catalytic Conversions of Synthesis Gas and Alcohols to Chemicals, Plenum Press, New York, London, 1984, p. 65.
[47] E.G. Baglin, G.B. Atkinson, L.J. Nicks, Ind. Eng. Chem., Prod. Res. Dev 20 (1981) 87–90.
[48] V.T. Coon, T. Takeshita, W.E. Wallace, R.S. Craig, J. Phys. Chem. 80 (1976) 1878–1879.
[49] J.B. Branco, D. Ballivet-Tkatchenko, A.P. de Matos, J. Phys. Chem. C 111 (2007) 15084–15088.
[50] JCPDS, The Powder Diffraction File, JCPDS, 1601 Park Avenue, Swarthmore, PA, 1981.
[51] V. Uvarov, I. Popov, Mater. Charact. 58 (2007) 883–891.
[52] A. Garbout, S. Bouattour, A.M.B. do Rego, A. Ferraria, A.W. Kolsi, J. Cryst. Growth 304 (2007) 374–382.
[53] D. Ballivet-Tkatchenko, G. Delahay, J. Thermal Anal. 41 (1994) 1141.
[54] D. Monti, A. Baiker, J. Catal. 83 (1983) 323–335.
[55] P. Mallet, A. Caballero, J. Chem. Soc., Faraday Trans. I 84 (1988) 2369.
[56] D. Ballivet-Tkatchenko, G. Delahay, J. Therm. Anal. 41 (1994) 1141–1151.
[57] C.D. Wagner, A.V. Naumkin, A. Kraut-Vass, J.W. Allison, C.J. Powell, J.R.R. Jr., NIST X-ray Photoelectron Spectroscopy Database, Standard Reference Database 20, Version 3.5, National Institute of Standards and Technology (NIST).
[58] L. Salvati, L.E. Makovsky, J.M. Stencel, F.R. Brown, D.M. Hercules, J. Phys. Chem. 85 (1981) 3700–3707.
[59] A.P. Grosvenor, M.C. Biesinger, R.S. Smart, N.S. McIntyre, Surf. Sci. 600 (2006) 1771–1779.
[60] K. Frohlich, R. Luptak, E. Dobrocka, K. Husekova, K. Cico, A. Rosova, M. Lukosius, A. Abrutis, P. Pisecny, J.P. Espinos, Mater. Sci. Semicond. Process. 9 (2006) 1065–1072.
[61] M. Houalla, C.L. Kibby, L. Petrakis, D.M. Hercules, J. Phys. Chem. 87 (1983) 3689–3693.
[62] C.S. Huang, M. Houalla, D.M. Hercules, C.L. Kibby, L. Petrakis, J. Phys. Chem. 94 (1990) 6749–6753.
[63] Vansante, W.M. Ra, Sachtler, J. Catal. 33 (1974) 202–209.
[64] D.D. Wagman, W.H. Evans, V.B. Parker, R.H. Schumm, I. Halow, S.M. Bailey, K.L. Churney, R.L. Nuttall, J. Phys. Chem. Ref. Data 11 (1982), Supplement 2.
[65] I. Barin, Thermochemical Data of Pure Substances, 3rd ed., VCH Verlagsgesellschaft mbH, Weinheim, New York, Basel, Cambridge, Tokyo, 1995.
[66] D.O. Bannikov, A.P. Safronov, N.A. Cherepanov, Thermochim. Acta 451 (2006) 22–26.
[67] S. Bennici, P. Carniti, A. Gervasini, Catal. Lett. 98 (2004) 187–194.
[68] B.C. Enger, R. Lodeng, A. Holmen, Appl. Catal. A 346 (2008) 1–27.
[69] A.G. Dedov, A.S. Loktev, I.I. Moiseev, A. Aboukais, J.F. Lamonier, I.N. Filimonov, Appl. Catal. A 245 (2003) 209–220.
[70] S. Kus, M. Otremba, M. Taniewski, Fuel 82 (2003) 1331–1338.
[71] J. Gouteron, D. Michel, A.M. Lejus, J. Zarembowitch, J. Solid State Chem. 38 (1981) 288–296.
[72] A.d. Andres, M.T. Fernandez-Diaz, J.L. Martinez, J. Rodriguez-Carvajal, R. Saez-Puches, F. Fernandezs, J. Phys.: Condens. Matter 3 (1991) 3813–3823.
[73] G. Adachi, N. Imanaka, Chem. Rev. 98 (1998) 1479–1514.
[74] C. Le Luyer, A. Garcia-Murillo, E. Bernstein, J. Mugnier, J. Raman Spectrosc. 34 (2003) 234–239.
[75] V. Grover, A. Banerji, P. Sengupta, A.K. Tyagi, J. Solid State Chem. 181 (2008) 1930–1935.
[76] G. Irmer, A. Dorner-Reisel, Adv. Eng. Mater. 7 (2005) 694–705.